Reaction of OH + NO_2 + M: A New View

David M. Golden*,† and Gregory P. Smith‡

Molecular Physics Laboratory, SRI International, Menlo Park, California 94025 and Department of Mechanical Engineering, Stanford University, Stanford, California 94305

Received: November 10, 1999; In Final Form: February 7, 2000

A reexamination of data and theoretical computations for the title reaction leads to the conclusion that both $HONO_2$ (nitric acid) and HOONO (pernitrous acid) can be formed. We describe hindered-Gorin RRKM calculations that fit most of the extant data and explain differences among the studies. We conclude that the rate constant for nitric acid formation at low temperatures could be considerably (∼20%) lower than the data for loss of OH in the presence of NO_2 would indicate. We have examined the atmospheric consequences of this conclusion on ozone and nitrogen oxide concentrations through the use of box models. We include a tentative recommendation for the rate constants for the individual steps as functions of temperature and density in the NASA format.

Introduction

The reaction of OH with NO_2 to form nitric acid ($HONO_2$)

$$HO + NO_2 + M \rightarrow HONO_2 + M \qquad (1)$$

is an effective chain-termination step in atmospheric chemistry, because HO_x and NO_x are sequestered in the reservoir species, nitric acid. (The "third body" M can be any of the molecules in the air.) Reaction 1 has long been known to be important and has been the subject of many studies, both experimental[1−15] and theoretical.[16−22] Models of chemical change in the atmosphere require a rate constant for this reaction as a function of temperature and density. Two often-quoted sources of this information are the NASA compilation (JPL 97-4 being the latest)[23] and the IUPAC[24] compilation. Unfortunately, these use somewhat different expressions for the rate constant as a function of temperature and density and list distinctly different values shown in Table 1.

NASA Format

$$k(\mathrm{M},T) = \left(\frac{k_0(T)[\mathrm{M}]}{1 + (k_0(T)[\mathrm{M}]/k_\infty(T))}\right) 0.6^{\{1+[\log(k_0(T)[\mathrm{M}]/k_\infty(T))]^2\}^{-1}} \qquad (2)$$

IUPAC Format

$$k(\mathrm{M},T) = \left(\frac{k_0(T)[\mathrm{M}]}{1 + (k_0(T)[\mathrm{M}]/k_\infty(T))}\right) \mathrm{Fc}^{\{1+[\log(k_0(T)[\mathrm{M}]/k_\infty(T))/(0.75-1.27\log(\mathrm{Fc}))]^2\}^{-1}} \qquad (3)$$

The most extensive laboratory data set has been obtained near 300 K. Figure 1 shows some of these data and the results of using the expressions for k(M) at 300 K in each of the aforementioned compilations.

The problem is not the different formats, but rather that the IUPAC recommendation has given great weight to the very high-pressure laboratory measurements, which, despite being out of the practical atmospheric range, were designed to help identify the high-pressure limit, whereas the NASA recommendation is a weighted fit to only the data below one atmosphere. This leads to significant differences in the 0.1−1 atm pressure range. In either case, some of the data are poorly fit.

In almost all cases, laboratory measurements involve following the loss of OH in the presence of fixed amounts of NO_2 and some bath gas, such as nitrogen or argon. In this paper, we posit that all of the experiments are correctly measuring the disappearance of OH, but that at least two products are formed, namely $HONO_2$ and HOONO (pernitrous acid). We explain, fit, and extrapolate the measurements using a simple form of RRKM theory with reasonable parameters. We examine the consequences of this finding on the atmosphere through the use of a box model.

Other workers have put forth the same suggestion.[7,9] In particular, Burkholder et al.,[9] in a very complete study, have delineated the limits for HOONO formation. We have performed detailed RRKM calculations, taking advantage of newer experimental results[11−15] and theoretical studies.[16−22] The results that we report here fall within the above limits.

Potential Energy Surface. The potential energy surface (PES) for this system has been theoretically examined in some detail.[17−19,22] It seems quite clear that HO and NO_2 react to form $HONO_2$ and HOONO. The latter is the intermediate for the important exothermic atmospheric reaction

$$HO_2 + NO \rightarrow HO + NO_2 \qquad (4)$$

Most studies suggest that HOONO is bound by about 20 kcal/mol at 0 K and that it exists in three conformers. HOONO has been observed in cold matrices by Lee and co-workers.[25] Figure 2 is a sketch of the PES, after Lin and co-workers,[20] but with the "critical energy for RRKM calculations", the energy at 0 K, set at 15.51 kcal/mol; the value that we find allows us to explain the data most satisfactorily. This corresponds to a bond dissociation energy at 300 K of 17 kcal/mol.

Kinetics. Given the two possible reaction products, we have performed RRKM calculations on the dissociation of each and,

† Department of Mechanical Engineering, Stanford University and Molecular Physics Laboratory, SRI International.

‡ Molecular Physics Laboratory, SRI International.

10.1021/jp9939928 CCC: $19.00
Published on Web 04/04/2000

TABLE 1: Comparison of NASA and IUPAC Parameters[a]

	low-pressure limit[b] $k_o(T) = k_o^{300}\,(T/300)^{-n}$			high-pressure limit[c] $k_\infty(T) = k_\infty^{300}\,(T/300)^{-m}$	
	k_o^{300}	n	Fc	k_∞^{300}	m
NASA (JPL 97−4)[a]	$(2.4 \pm 0.2) \times 10^{-30}$	3.1 ± 0.2	0.6	$(1.7 \pm 0.2) \times 10^{-11}$	2.1 ± 0.3
IUPAC	2.6×10^{-30}	2.9	$\exp(-T/340)$	7.5×10^{-11}	0.6

[a] JPL 97-4 values have been corrected to reflect proper weighting of the data, assuming that all measurements reflect nitric acid as the only product. (In JPL 97-4 the recommended parameters reflected an unweighted fitting of the data. This caused significant changes from earlier recommendations at 220 K. The parameters in Table 1 represent a weighted fit to the data, using reported error limits as the weights.) The values quoted are suitable for N_2 as the third body, M. [b] Units are cm^6/molecule^2-sec. [c] Units are cm^3/molecule-sec.

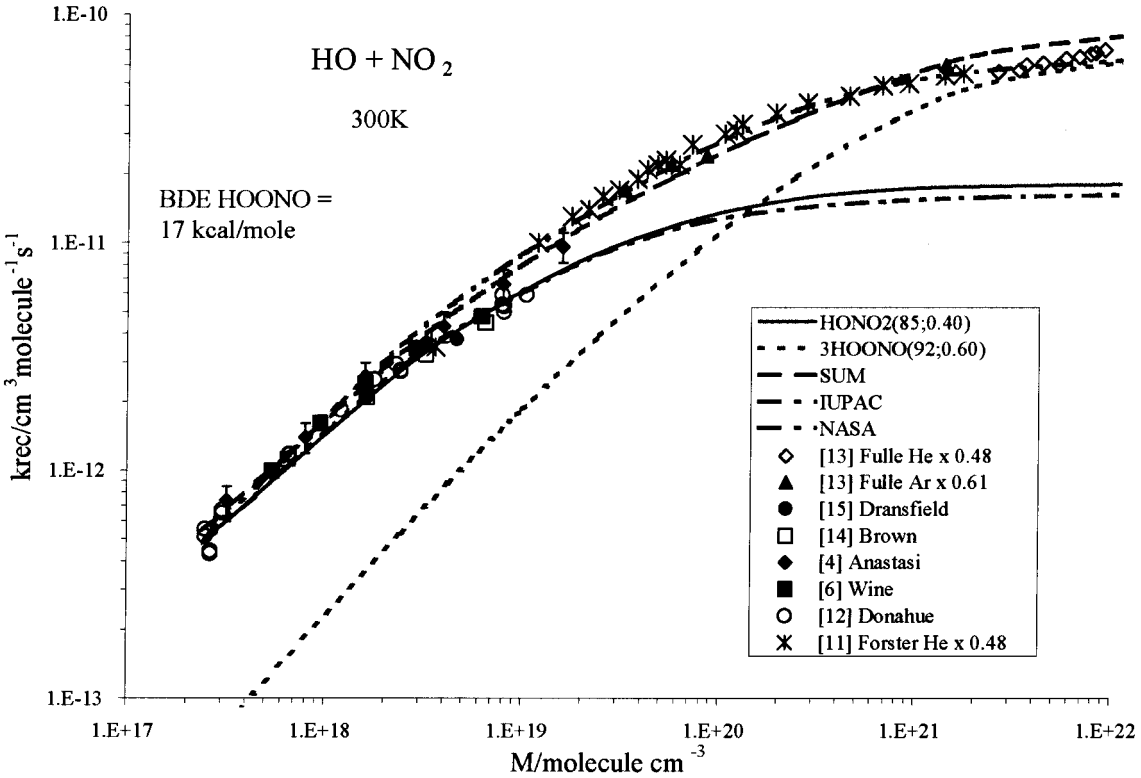

Figure 1. Rate constant as a function of N_2 density at 300 K. The measured points all reflect OH loss measurements. The lines labeled IUPAC and NASA are from the parameters in Table 1. Densities for experiments in He have been scaled by 0.48 and those in Ar by 0.61. The lines labeled $HONO_2$ and HOONO are the results of RRKM calculations described in the text. The numbers in parentheses after $HONO_2$ and HOONO are the hindrance parameter and collisional efficiency, respectively (see text.). The line labeled sum is the sum of the RRKM calculations for the two channels. (Note that sum and IUPAC overlap, and NASA and $HONO_2$ essentially do also.)

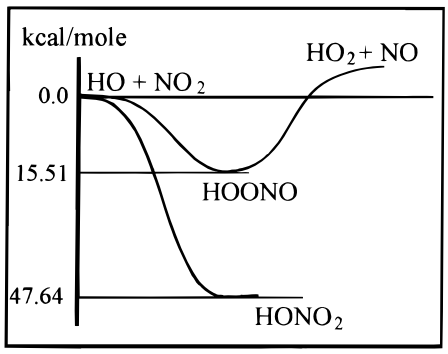

Figure 2. Schematic potential energy surface.

with the appropriate equilibrium constants, have calculated the rate of formation of each from HO and NO_2. The observed rate constant is the sum of these separate pathways, provided that the less stable isomer has a lifetime long compared with the experimental time. Otherwise, the less stable isomer will decompose on the time scale of the experiment, and only the formation of the more stable isomer will be measured. (We do not allow for isomerization of HOONO to $HONO_2$. The theoretical barrier is greater than 40 kcal/mol.[19])

RRKM Calculations. The RRKM calculations were carried out as set forth in our 1978 paper.[16] We treated the transition states using the "hindered-Gorin" model. In the Gorin model, the transition state is treated as if OH and NO_2 were not covalently bonded but completely free to rotate. (At a micro-canonical level, this is equivalent to phase space theory.) We have noted that if the OH and NO_2 species were placed at a distance apart corresponding to the centrifugal maximum in a Lennard−Jones attractive potential, they would collide as they rotated, considering their van der Waals radii. Thus, we characterize the tightness of the transition state using the hindrance parameter η, described in Smith and Golden,[16] as the percentage of the 4π steradians unavailable to the rotating species. In effect, we are treating the rotations by varying the rotational level spacing through use of η, thereby controlling the entropy and heat capacity of the transition state. The hindrance is introduced into the RRKM code by multiplying the adiabatic two-dimensional rotor moments of inertia of the

TABLE 2: Rate Constants/cm^{3}Molecules^{-1} s^{-1} vs Density at 300 and 220 K

300 K					
M/molecules cm^{-3}	*k*(HNO3)	*k*(HOONO)	sum	*k*/IUPAC	*k*/NASA
2.44×10^{17}	4.90×10^{-13}	$5.89 \times 10-14$	5.49×10^{-13}	5.00×10^{-13}	4.82×10^{-13}
2.44×10^{18}	2.75×10^{-12}	5.31×10^{-13}	3.28×10^{-12}	3.54×10^{-12}	2.86×10^{-12}
7.72×10^{18}	5.40×10^{-12}	1.49×10^{-12}	6.89×10^{-12}	7.66×10^{-12}	5.32×10^{-12}
1.00×10^{19}	6.16×10^{-12}	1.87×10^{-12}	8.02×10^{-12}	8.90×10^{-12}	6.04×10^{-12}
2.44×10^{19}	9.04×10^{-12}	3.90×10^{-12}	1.29×10^{-11}	1.43×10^{-11}	8.87×10^{-12}
7.72×10^{19}	1.28×10^{-11}	9.25×10^{-12}	2.20×10^{-11}	2.48×10^{-11}	1.22×10^{-11}
2.44×10^{20}	1.55×10^{-11}	1.94×10^{-11}	3.50×10^{-11}	3.81×10^{-11}	1.42×10^{-11}
7.72×10^{20}	1.71×10^{-11}	3.45×10^{-11}	5.15×10^{-11}	4.95×10^{-11}	1.53×10^{-11}
2.44×10^{21}	1.77×10^{-11}	5.07×10^{-11}	6.84×10^{-11}	5.73×10^{-11}	1.58×10^{-11}
2.44×10^{22}	1.82×10^{-11}	6.75×10^{-11}	8.57×10^{-11}	6.55×10^{-11}	1.64×10^{-11}
220K					
M/molecules cm^{-3}	*k*(HNO3)	*k*(HOONO)	sum	*k*/IUPAC	*k*/NASA
3.33×10^{17}	1.23×10^{-12}	2.14×10^{-13}	1.44×10^{-12}	1.70×10^{-12}	1.59×10^{-12}
3.33×10^{18}	5.37×10^{-12}	1.67×10^{-12}	7.04×10^{-12}	1.06×10^{-11}	7.79×10^{-12}
1.05×10^{19}	8.95×10^{-12}	4.41×10^{-12}	1.34×10^{-11}	2.04×10^{-11}	1.37×10^{-11}
1.37×10^{19}	9.81×10^{-12}	5.42×10^{-12}	1.52×10^{-11}	2.32×10^{-11}	1.53×10^{-11}
3.33×10^{19}	1.26×10^{-11}	1.06×10^{-11}	2.32×10^{-11}	3.55×10^{-11}	2.07×10^{-11}
1.05×10^{20}	1.53×10^{-11}	2.26×10^{-11}	3.79×10^{-11}	5.34×10^{-11}	2.57×10^{-11}
3.33×10^{20}	1.68×10^{-11}	4.16×10^{-11}	5.84×10^{-11}	6.72×10^{-11}	2.85×10^{-11}
1.05×10^{21}	1.74×10^{-11}	6.39×10^{-11}	8.13×10^{-11}	7.54×10^{-11}	2.99×10^{-11}
3.33×10^{21}	1.76×10^{-11}	8.24×10^{-11}	1.00×10^{-10}	8.01×10^{-11}	3.07×10^{-11}
3.33×10^{22}	1.80×10^{-11}	1.03×10^{-10}	1.21×10^{-10}	8.48×10^{-11}	3.15×10^{-11}

OH and NO_2 fragments in the transition state each by $(1 - \eta)^{1/2}$. The frequencies of $HONO_2$ are known,[16] and those of HOONO are taken from a combination of theory and experiment.[20] The moments of inertia are computed from molecular structures. Details of the parameters for calculations of both channels are given in the Appendix.

Values for η and β (the collision efficiency) at 300 K for $HONO_2$ were chosen to obtain agreement with the laboratory data. An η_{300} of 85% arises from fitting the data at a density of 1×10^{19} molecules cm^{-3}, whereas the β_{300} value of 0.4 comes from fitting the low-pressure data. The data near one atmosphere are assumed to be due only to $HONO_2$ formation, because HOONO decomposes rapidly under these conditions (from ~150 ms at 10 Torr to 3 ms at 1 atm), and at low pressure, the most stable isomer will dominate (see Figure 1). Values of η and β at 300 K for HOONO were chosen to fit the data at the highest pressure and in the falloff region near one atmosphere, respectively. The values at 220 K were computed by increasing the moments of inertia of the transition states according to a Lennard−Jones attractive potential, keeping the hindrances essentially constant in both channels and allowing the collision efficiency to increase slightly, as expected. See the Appendix for details on the RRKM parameters. HOONO was given a degeneracy of three to account for three nearly energetically identical isomers.[19]

Results

Table 2 displays the computed rate constants for the combination of OH and NO_2 to each isomer, as well as their sum, for a series of densities at 300 K and 220 K. Figure 1 shows the 300 K data and computations and Figure 3 shows the 220 K data and computations. The IUPAC recommendation and the NASA recommendation (using the parameters in Table 1, which are corrected from JPL 97−4 by weighting the data properly at 220 K) that is a fit to the data ignoring the high-pressure values at 300 K are also shown.

At 300 K, the values of the rate constant at the higher densities (1×10^{19} molecules cm^{-3}) reflect the fact that a large contribution to OH loss could come from the formation of HOONO. In these experiments,[11,13] OH loss was measured on a microsecond time scale, whereas the computed lifetime of HOONO ranges from ~3 ms at 1 atm to ~0.2 ms at 100 atm. Figure 3 illustrates that there can be contributions from the formation of HOONO at all densities at 220 K. This means that the rate constant for $HONO_2$ formation could be less than suggested by NASA or IUPAC, and HOONO may live long enough to either photolyze or react with OH.

The measured rate-constant values at the lower densities at 300 K correspond only to the formation of nitric acid because HOONO formed under these conditions, at 300 K and at densities near 1×10^{19} molecules cm^{-3}, has a lifetime that is shorter than the experimental observation times. Thus, HOONO decomposes back to OH, and the only observed loss pathway is nitric acid formation. For experiments at the higher densities and the lower temperature, HOONO is stable and both pathways contribute to the observed OH loss. There is one 300 K point from Forster et al.,[11] at a density of 3.65×10^{18} with a value of $k = 3.5 \times 10^{-12}$, that falls on the nitric acid line, although this experiment should measure both channels. This may reflect some error in that experiment. Also, the highest pressure point, from Brown et al.,[14] is for a pressure at which the lifetime of HOONO would be about 7 ms, according to our calculations. The experimental time is on the order of 0.4 ms, so either that one point is in error or the bond strength of HOONO would have to be lowered to 16 kcal mol^{-1}, corresponding to a lifetime for HOONO of 0.2 ms. In this case, the values of η and β would have to change to somewhat less-conventional values, and the contribution of HOONO formation to the disappearance of OH in the presence of NO_2 at 220 K will be somewhat reduced as well. There are three other experiments in the intermediate pressure range for which the HOONO lifetime is relevant to their interpretation. The points from Anastasi and Smith[4] have error limits that split the differences between the two curves, but their experiment was carried out with lifetimes of approximately 0.1 ms, so their data likely represent the sum of both pathways. The other measurements, Wine et al.,[6] whose highest data points correspond to a lifetime in the range of 5 ms, and the Harvard flow experiments[12,15] of 50 ms duration should correspond to nitric acid formation only.

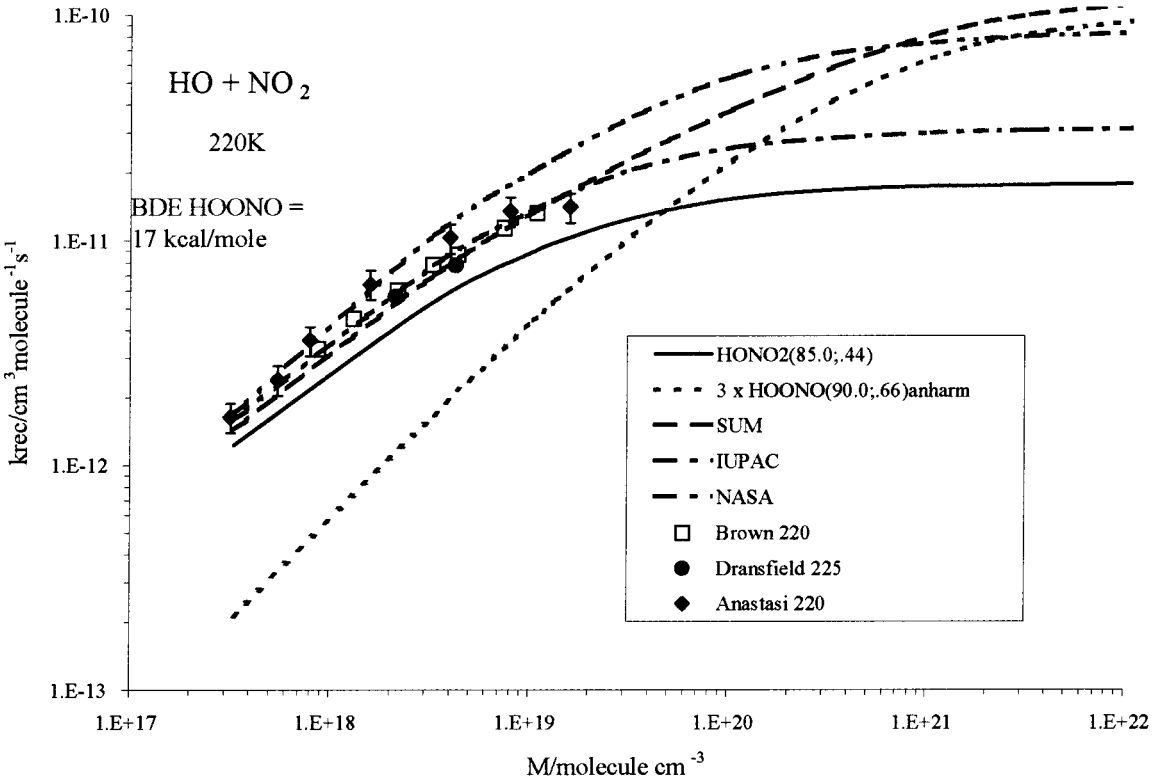

Figure 3. Rate constant at 220 K as a function of N_2 density, as in Figure 1.

Discussion

Transition States and RRKM Calculations. The hindered-Gorin method, used here, has been used by us for many years to characterize experimental systems. More detailed microcanonical variational methods may be employed along with master equation formalisms,[26] but the uncertainties in the underlying PES and the methods themselves justify our current simple semiempirical approach to this problem. The energy-transfer parameter that we have used for the N_2 bath gas is reasonably consistent with the literature. The NASA and IUPAC compilations make use of similar values. The hindrance parameter essentially fixes the high pressure limiting value of the rate constant to be less than the Gorin limit, a frequently shared conclusion.

There are several combinations of the parameters at our disposal that allow the RRKM calculations to fit the data. Different values (± 2 kcal/mol) of the bond energy (hence lifetime) in HOONO lead to different hindrances and collisional efficiencies. Only a very accurate PES, combined with a code sufficiently detailed to take into account anharmonicities, internal rotors, the physics of energy transfer, and other fine points, could eliminate some of the choices. Our selection of parameters (β, η, and bond strength) employs typical and reasonable values that are consistent with a good fit to the data and the HOONO lifetimes required for the interpretation of these data.

Among the somewhat arbitrary aspects of the calculations that we present here are the fixing of the transition state adiabatic moments of inertia by using the Lennard−Jones attractive potential. We then float the hindrance and collision efficiency to fit the data. The high-pressure data are more sensitive to the former and the low-pressure data are more sensitive to the latter. (We could, and have, varied these values within reason, but the conclusions are unchanged.) If we are to accept all of the data at 300 K, along with the scaling for He and Ar of 0.48 and 0.61, respectively, as given by Donahue et al.,[12] and the general result that those experiments performed at lower densities were carried out over a time longer than the HOONO lifetime at 300 K, whereas those at the higher densities were not, we are fairly well constrained in our parameter choice. (These scaling factors are in keeping with a large body of data[23,24] on the relative collisional efficiencies of N_2, He and Ar bath gases.) Input parameters to the RRKM code are given explicitly in the Appendix.

TABLE 3: Parameters for $HONO_2$ and HOONO Formation (NASA Format)

	low-pressure limit $\lvert k_0(T) = k_0^{300}\,(T/300)^{-n}$			high-pressure limit $\lvert k_\infty(T) = k_\infty^{300}\,(T/300)^{-m}$	
	k_0^{300}	n	Fc	k_∞^{300}	m
$HONO_2$	2.4×10^{-30}	2.6	0.6	1.8×10^{-11}	0.1
HOONO	2.3×10^{-31}	3.1	0.6	7.3×10^{-11}	1.3

If we were willing to discount the high-pressure data at 300 K and the theoretical computations, we could argue that the HOONO isomer is not formed (i.e., it is much less stable than the theoretical calculations suggest) and that the curves for nitric acid formation in Figure 1 can be extrapolated to higher densities. Then, we can fit the data at 220 K asserting that only nitric acid is formed. Under those conditions, changing the hindrance to 65% and lowering the bond energy in HOONO substantially will also reproduce the data. Therefore, this would argue that the values in Table 1 from the NASA compilation should be used.

Rate Constants for Atmospheric Modeling. We conclude that the values to be used for the reaction of OH with NO_2 in the atmosphere must take into account two distinct pathways. The values in the NASA format for the formation of $HONO_2$ and HOONO are given in Table 3. It should be kept in mind that the parameters representing the high and low pressure limiting rate constants are somewhat different than those that come directly from the RRKM model. The NASA expression is simply an analytical three parameter (k_0, k_∞, and Fc) fit to the

curve predicted by RRKM calculations with the additional constraint that the curvature is being forced through the use of Fc = 0.6 in fitting the RRKM results. There is a good deal of uncertainty in the ratio of $HONO_2$ to HOONO production. In addition, although the largest effect on atmospheric model results is the lowering of the nitric acid formation rate constant, the HOONO photolysis, decomposition, and reaction with OH should also be added to the models. We suggest using $HOONO_2$ as a surrogate for photolysis and OH reaction rates. The decomposition rate can be calculated from the equilibrium constant. Using the format of Table 3 in JPL 97−4, K/cm^3 molecule^{-1} = A exp(B/T) with $A = 1.2 \times 10^{-26}$; $B = 8260$; K(298 K) = 1.3×10^{-14}, K (220 K) = 2.4×10^{-10} and the multiplicative uncertainty at 298 K, f(298 K) = 10. (This value of the equilibrium constant reflects the degeneracy of three for HOONO.)

Implications for Atmospheric Models. We have examined the implications of an OH + NO_2 → HOONO product channel on global photochemical models of the atmosphere, using box models derived for various locations from the LLNL diurnally averaged 2-D model.[27] Details of the process may be found in papers describing a local sensitivity−uncertainty analysis performed using this methodology.[28,29] The local rate parameters are extracted for specific latitude, altitude, and season for 155 reactions and photolysis processes, representing the photochemistry of the stratosphere and free troposphere. The JPL-94 rate parameters were used.[30] We added three HOONO loss processes, the decomposition rate constant from the RRKM calculations, and the photolysis and OH reaction at the same rates as pernitric acid, subject to high uncertainty. The Sandia code Senkin[31] was used to integrate the kinetics to convergence, and also returns sensitivity coefficients $S_{ij} = (dX_i/X_i)/(dk_j/k_j)$ describing the relative change in model concentration given a relative change in rate parameter, j.

The 2-D model outputs that serve as initial concentrations deviate from a local photostationary state (except in the upper stratosphere) because of fluxes from other locations and times in the seasonally varying model, and this is reflected in local production minus loss (P − L) rates in the 2-D model output. We can add up various family P − L terms (NO_x, Cl_x, Br_x, HO_x, and O_3) and include a smaller net first-order rate term in the mechanism to freeze the solution in the box to the 2-D values.[28,29] Thus, each family total concentration remains fixed. The net fluxes are assigned to the terms with the largest individual P − L flux in the appropriate direction, and we generally compute small sensitivities for ozone to these terms. The locations were selected for this comparative rate examination and their uncomplicated and insensitive P − L treatments; they provided steady converged solutions for cases in which the OH + NO_2 rates were altered. The long-lived trace gases (H_2O, CH_4, N_2O, CFCs, etc.) were kept constant. The box-model runs are integrated in time until concentrations and sensitivities converge to final values (two months to two years).

Guided by the previous ozone-sensitivity analysis to OH + NO_2, we selected a small representative sample of four local boxes to examine: March in the subtropics at 32 N and 31 km, two northern summer locations at 62 N and 25 km and 31 km in August, and an upper tropospheric box at 62 N and 10 km in August. Temperatures are 220−230 K and pressures vary from 10 to 200 Torr. Original box-model runs were compared to runs in which a fraction of the $HONO_2$ production-rate constant is replaced by the new branching fraction predicted from the OH + NO_2 → HOONO calculation. The total rate constant for OH + NO_2 is kept the same, and only the product fraction is changed. The results are shown in Table 4. Note the first run required no net P − L rate terms.

TABLE 4: Model Results from Including HOONO Chemistry

location	P − L terms	% HOONO formation	ΔO_3	sensitivity prediction	ΔNO_x
32 N Mar 31 km	none	16	−0.020	−0.021	+0.055
62 N Aug 31 km	O_3, NO, Cl, Br, H_2O_2	16	−0.026	−0.027	+0.063
62 N Aug 25 km	O_3, NO, Cl, Br, OH	19	−0.033	−0.033	+0.116
62 N Aug 10 km	O_3, NO_2, HCl, BrO, OH	31	+0.077	+0.074	+0.265

The model runs demonstrate a 3% ozone decrease in the midstratosphere as a consequence of 17% formation of the HOONO isomer from OH + NO_2, and furthermore, a 10% absolute uncertainty in this yield implies a 2% uncertainty in predicted local ozone. In the cold upper troposphere, at higher pressure, the branching fraction and effect on ozone are larger and in the opposite direction. One can see in both cases that the ozone change is the same as we predict in column 5 using the original box-model sensitivity to the OH + NO_2 → $HONO_2$ reaction, which means that the effect is simply due to a lesser formation rate for nitric acid. In all of the runs with the HOONO kinetics added, ozone sensitivity to these specific rate-constant values was negligible, whereas values of 0.15 are typical for OH + NO_2 → $HONO_2$ at 31 km. The HOONO concentrations are less than 0.02% of $HONO_2$, and the HOONO half-life, due to its thermal decomposition in the model, is several minutes. Therefore, HOONO is too short-lived to function as a reservoir.

The opposite effect of diminished nitric acid formation on ozone below the tropopause can be attributed to the active role of NO_2 photochemistry in the troposphere. Above 20 km, nitric acid removes species from both HO_x and NO_x catalytic ozone destruction cycles. At 10 km, there is a large sensitivity (+0.25) to NO_2 photolysis, which produces ozone via photochemical oxidation of hydrocarbons. Hence, reducing NO_2 sequestration in nitric acid will increase ozone. We also see, from the RRKM rate constants and Table 4, that the largest and observationally noticeable predicted effects occur in the cold troposphere, in which the higher pressures have increased the yields of HOONO. Finally, although the HOONO loss rates are quite uncertain, the predicted half-lives (with bond strengths of 17 kcal/mol) are too short for the concentration to build up as a nighttime reservoir species and serve as a daylight photolytic HO_x source after sunrise. (HONO photolysis has been suggested as a sunrise OH source.[32])

In a recent paper, Osterman et al.[33] observed NO_x(=NO + NO_2)/NO_y ratios from 8 to 38 km at 65 N in early summer, but modeling significantly underpredicts this ratio. They suggest a 20% or more reduction in the OH + NO_2 → $HONO_2$ rate constant (from JPL-94) to correct this stratospheric discrepancy. A significant HOONO channel will have the same effect. The final column of Table 4 shows 6−12% increases in stratospheric NO + NO_2 from the HOONO kinetics runs. Note that much larger changes in NO_x occur for the 10 km model runs. The low-altitude data are less precise but do not show large disagreement with model results. The sensitivity of the title reaction to simulations of arctic winter has also been recently discussed.[34]

These predicted effects may be smaller in a 2-D model at the lower altitudes due to effects of transport and radiation increases from the lower overhead ozone. Decreases of 30−

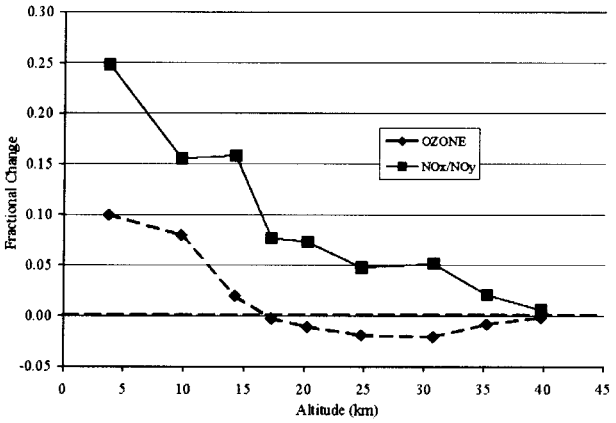

Figure 4. Sensitivity analysis estimate of the effect of HOONO formation at 47 N Aug; fractional changes as a function of altitude: squares, NO*x*; diamonds, O_3.

60% have been seen in some cases.[28,29] The recent 2-D model study by Partmann et al.[35] altered three rate constants including OH + NO_2. However, much smaller ozone changes were predicted below 15 Km than the box model sensitivities would suggest.

Other concentration changes were also seen in the 4 runs with HOONO chemistry. The OH concentrations increase and those of HO_2 decrease slightly, and of course, nitric acid dropped, −10%. The several percent increase in NO_2 in turn decreases ClO, with which it reacts. The most notable change in the stratospheric model predictions is a 10% decrease in H_2O_2. One additional feature, noted at 10 km, is a 30% increase in predicted $ClONO_2$, following a similar rise in NO_2. The stratospheric model $ClONO_2$ is relatively unchanged.

Figure 4 shows an altitude profile of the predicted effects of the HOONO channel on O_3 and NO*x* derived from our sensitivity analysis results[28,29] at 47 N in August. The trends seen for the selected full box model computations at 62 N hold here as well, at slightly smaller magnitude. In the lower altitudes of the troposphere, the HOONO branching fraction decreases as the temperature increases but increases as the pressure rises. Its predicted local effects remain high due to continued sensitivity to the OH + $NO_2 \rightarrow HONO_2$ rate constant. At 300 K and 1 atm, the predicted HOONO branch is 30%, so one may expect regional air models and smog-chamber simulations to be similarly sensitive to this mechanistic modification,[36] although HOONO will rapidly redecompose at this temperature.

Conclusion

RRKM calculations suggest that the data reported for the disappearance of OH in the presence of NO_2 represent the sum of at least two chemical reactions. This implies that the currently accepted values for the rate constant for nitric acid formation from these species are too high. For cases in which an appropriately lower value for the nitric acid forming step is used, atmospheric models show a significant change in ozone and NO_x values. Stratospheric concentrations are particularly affected by the lowering of the nitric acid formation rate constant at the low temperatures. At 300 K, the differences between the NASA values, which are preferred, and the IUPAC values also have important consequences for tropospheric models and in the understanding of smog-chamber experiments.

Appendix

TABLE 5: Inputs for the RRKM Calculations

$HONO_2$	
critical energy at 0 K/kcal mol^{-1}	47.64
frequencies/cm^{-1}	3560, 1710, 1335, 1320, 886, 765, 680, 583, 465
dissociation energies for anharmonicities/kcal mol^{-1}	107, 48, 72, 72, 72, 48, 107, 372, 348
product of adiabatic moments of inertia/$10^{80}gm^2$ cm^4	9.38×10^3
moment of inertia: active external rotor/10^{40}gm cm^2	63.85
HO- - -NO_2 (Transition State)	
frequencies	3730, 1620, 1320, 750
dissociation energies for anharmonicities/kcal mol^{-1}	104, 45, 45, 345
$I^{\#}/I_{300}$; $I^{\#}/I_{220}$	7.83; 8.68
product of adiabatic moments of inertia/$10^{80}gm^2$ cm^4	$5.75 \times 10^5 \times$ at 300 K; 7.07×10^5 at 220 K
moment of inertia: active external rRotor/10^{40}gm cm^2	63.85
moment of inertia: active 2-D rotors/$10^{80}gm^2$ cm^4	1.45($\sigma = 1$); 15.51($\sigma = 2$)
β300; β220; η300;η220	0.40; 0.44; 85%; 85%
HOONO	
critical energy at 0 K/kcal mol^{-1}	15.51
frequencies/cm^{-1}	3748, 1823, 1407, 1014, 808, 459, 358, 293, 212
dissociation energies for anharmonicities/kcal mol^{-1}	100, 120, 24, 16, 24, 40, 24, 300, 300
product of adiabatic moments of inertia/$10^{80}gm^2$ cm^4	3.22×10^4
moment of inertia: active external rotor/10^{40}gm cm^2	14.38
HO- - -ONO (transition state)	
frequencies	3730, 1620, 1320, 750
dissociation energies for anharmonicities/kcal mol^{-1}	104, 45, 45, 345
$I^{\#}/I_{300;}$ $I^{\#}/I_{220}$	5.39; 5.97
product of adiabatic moments of inertia/$10^{80}gm^2$ cm^4	9.34×10^5 at 300 K; 1.15×10^6 at 220 K
moment of inertia: active external rotor/10^{40}gm cm^2	14.38
moment of inertia: active 2-D rotors/$10^{80}gm^2$ cm^4	1.45($\sigma = 1$); 32.67($\sigma = 2$)
β300; β220; η300; η220	0.40; 0.44; 95%; 95%

Table 5 shows the inputs for the RRKM calculations for $HONO_2$ and HOONO. Structures, frequencies, and heats of formation for $HONO_2$ and HOONO were taken mostly from Smith and Golden[16] and Chakraborty et al.[20] Because the theoretical calculations[19] suggest that there are three almost energetically equal isomers of HOONO, a degeneracy of three was used in computing the equilibrium constant for its formation from HO and NO_2. We applied anharmonicities to the frequencies somewhat arbitrarily. Our code allows the input of a bond energy associated with each frequency. It then computes anharmonicities via the Birge−Sponer relationship[37] ($\chi_0 = \omega_0/4D_0$). We allowed stretching frequencies to be associated with the bond strengths of the involved bonds and used high values for the bending vibrations. The frequencies in the transition states are those of OH and NO_2. The active external rotors in the molecules are the K-rotors essentially around the axis of the breaking bond, here characterized by the smallest moment of inertia. The same values are used for the transition states. The active two-dimensional "Gorin-rotors" in the transition states are ascribed to the OH and NO_2 species. The OH value is the value for OH radical. The NO_2 two-dimensional moment of inertia values are arrived at by forcing the NO_2 product of

inertia to be equal to 15 350 $\times$ 10^{-120} gm·cm^2. This is divided by the value used for the active one-dimensional K-rotor, and the square root of that number is the moment of inertia for the two-dimensional NO_2 rotors in the hindered-Gorin transition state. The adiabatic moments of inertia in the molecules are computed from structures. The adiabatic moments of inertia in the transition states are computed from those in the molecule using the Lennard−Jones attractive potential for a pseudodiatomic system, viz:

$$I^{\#}/I = (6\Delta H_0/RT)^{1/3} \quad (5)$$

The values of $I^{\#}$ and I in this equation represent two-dimensional rotors. The value of $I^{\#}/I$ above is used in the Waage−Rabinovitch correction for the effects of rotational energy on the value of the rate constants.

The β_{300} value for $HONO_2$ came from fitting the lowest pressure values of the rate constants. A higher β_{300} value for HOONO was adopted in order to better fit the pressure dependence above one atmosphere. The β_{220} values represent an increase of 10% as the temperature decreases. (A strict use of the formula used by NASA and IUPAC would yield a 17% increase, which could probably be accommodated by appropriate changes in hindrance, but the values used provide a slightly better representation of the data.) The η_{300} values were determined by fitting the data. The η_{220} values were fitting parameters as well, but they were kept constant ($HONO_2$) or made slightly lower (HOONO) than the values at 300 K because the transition state should get somewhat looser as the centrifugal barrier moves to larger distances at lower temperatures.

Acknowledgment. This work was supported by NASA Contract NAG2-955 with the Upper Atmosphere Research Program, Contract 961440 with the Atmospheric Effect of Aircraft Program to SRI International, and a gift from the Dow Chemical Co. to Stanford University for support of D.M.G.

References and Notes

(1) Anderson, J. G.; Margitan, J. J.; Kaufman, F. *J. Chem. Phys.* **1974**, *60*, 3310−3317.
(2) Howard, C. J.; Evenson, K. M. *J. Chem. Phys.* **1974**, *61*, 1943−1952.
(3) Harris, G. W.; Wayne, R. P. *J. Chem. Soc., Faraday Trans.* **1975**, *1*, 610−617.
(4) Anastasi, C.; Smith, I. W. M. *J. Chem. Soc., Faraday Trans. 2* **1976**, *72*, 1459−1468.
(5) Erler, K.; Field, D.; Zellner, R.; Smith, I. W. M. *Ber. Bunsen-Ges. Phys. Chem.* **1977**, *81*, 22−26.
(6) Wine, P. H.; Kreutter, N. M.; Ravishankara, A. R. *J. Phys. Chem.* **1979**, *83*, 3191−3195.
(7) Robertshaw, J. S.; Smith, I. W. M. *J. Phys. Chem.* **1982**, *86*, 785−790.
(8) Burrows, J. P.; Wallington, T. j.; Wayne, R. P. *J. Chem. Soc., Faraday Trans. 2* **1983**, *79*, 111−122.
(9) Burkholder, J. R.; Hammer, P. D.; Howard, C. J. *J. Phys. Chem.* **1987**, *91*, 2136−2144.
(10) Bossard, A. R.; Singleton, D. L.; Paraskevopoulos, G. *Int. J. Chem. Kinet.* **1988**, *20*, 609−620.
(11) Forster, R.; Frost, M.; Fulle, D.; Hamann, H. F.; Hippler, H.; Schlepegrell, A.; Troe, J. *J. Chem. Phys.* **1995**, *103*, 2949−2958.
(12) Donahue, N. M.; Dubey, M. K.; Mohrschladt, R.; Demerjian, K. L.; Anderson, J. G. *J. Geophys. Res.* **1997**, *102*, 6159−6168.
(13) Fulle, D.; Hamann, H. F.; Hippler, H.; Troe, J. *J. Chem. Phys.* **1998**, *108*, 5391−5397.
(14) Brown, S. S.; Talukdar, R. K.; Ravishankara, A. R. *Chem. Phys. Lett.* **1999**, *299*, 277-.
(15) Dransfield, T. J.; Perkins, K. K.; Donahue, N. M.; Anderson, J. G.; Sprengnether, M. M.; Demerjian, K. L. *Geophys. Res. Lett.* **1999**, *26*, 687−690.
(16) Smith, G. P.; Golden, D. M. *Int. J. Chem. Kinet.* **1978**, *10*, 489−501.
(17) McGrath, M. P.; Francl, M. M.; Rowland, F. S.; Hehre, W. J. *J. Phys. Chem.* **1988**, *92*, 5352−5357.
(18) McGrath, M. P.; Rowland, F. S. *J. Phys. Chem.* **1994**, *98*, 1061−1067.
(19) Sumathi, R.; Peyerimhoff, S. D. *J. Chem. Phys.* **1997**, *107*, 1872−1880.
(20) Chakraborty, D.; Park, J.; Lin, M. C. *Chem. Phys.* **1998**, *231*, 39−49.
(21) Doclo, K.; Röthlisberger, U. *Chem. Phys. Lett.* **1998**, *297*, 205−210.
(22) Jitariu, L. C.; Hirst, D. M. *Phys. Chem. Chem. Phys.* **1999**, *1*, 983−987.
(23) DeMore, W. B.; Sander, S. P.; Golden, D. M.; Hampson, R. F., Jr.; Kurylo, M. J.; Howard, C. J.; Ravishankara, A. R.; Kolb, C. E.; Molina, M. J. "*Chemical Kinetics and Photochemical Data for Use in Stratospheric Modeling*," NASA/JPL: Pasadena, 1997.
(24) Atkinson, R.; Baulch, D. L.; Cox, R. A.; Hampson, R. F., Jr.; Kerr, J. A.; Rossi, M. J.; Troe, J. *J. Phys. Chem. Ref. Data* **1999**, *28*, 191−393.
(25) Cheng, B. M.; Lee, J. W.; Lee, Y. P. *J. Phys. Chem.* **1991**, *95*, 2814.
(26) Holbrook, K. A.; Pilling, M. J.; Robertson, S. H. *Unimolecular Reactions*; John Wiley & Sons Ltd.: Chichester UK, 1996.
(27) Wuebbles, D.; Connell, P. S.; Grant, K.; Kinnison, D. E.; Rotman, D. *The Atmospheric Effects of Stratospheric Aircraft: Report of the 1992 Models and Measurements Workshop*; Remsberg, M. J. P. a. E. R., Ed.; NASA: Washington D. C., 1993.
(28) Dubey, M. K.; Smith, G. P.; Hartley, W. S.; Kinnison, D. E.; Connell, P. S. *Geophys. Res. Lett.* **1997**, *24*, 2737−2741.
(29) Dubey, M. K.; Smith, G. P.; Kinnison, D. E.; Connell, P. S., in preparation.
(30) DeMore, W. B.; Sander, S. P.; Golden, D. M.; Hampson, R. F., Jr.; Kurylo, M. J.; Howard, C. J.; Ravishankara, A. R.; Kolb, C. E.; Molina, M. J. "*Chemical Kinetics and Photochemical Data for Use in Stratospheric Modeling*," NASA/JPL: Pasadena, 1994.
(31) Lutz, A. E.; Kee, R. J.; Miller, J. A. "SENKIN: A Fortran Program for Predicting Homogeneous Gas-Phase Chemical Kinetics with Sensitivity Analysis," Sandia National Laboratories, 1988.
(32) Wennberg, P. O.; Cohen, R. C.; Stimpfle, R. M.; Koplow, J. P.; Anderson, J. G.; Salawitch, R. J.; Fahey, D. W.; Woodbridge, E. L.; Keim, E. R.; Gao, R. S.; Webster, C. R.; May, R. D.; Toohey, D. W.; Avallone, L. M.; Proffitt, M. H.; Loewenstein, M.; Podolske, J. R.; Chan, K. R.; Wofsy, S. C. *Science* **1994**, *266*, 398−404.
(33) Osterman, G. B.; Sen, B.; Toon, G. C.; Salawitch, R. J.; Margitan, J. J.; Blavier, J. F.; Fahey, D. W.; Gao, R. S. *Geophys. Res. Lett* **1999**, in press.
(34) Ruhnke, R.; Kouker, W.; Reddmann, T. *J. Geophys. Res.* **1999**, *104*, 3755−3772.
(35) Partmann, R. W.; Brown, S. S.; Gievczak, T.; Talukdar, R. K.; Burkholder, J. B.; Ravishankara, A. R. *Geophys. Res. Lett.* **1999**, *26*, 2387−2390.
(36) Tonnesen, G. S. *Atmos. Environ.* **1999**, *33*, 1587−1598.
(37) Herzberg, G. *Molecular Spectra and Molecular Structure: I. Spectra of Diatomic Molecules*; D. Van Nostrand co. Inc.: Princeton, NJ, 1950.